# Regulating the reaction zone of electrochemical $CO_2$ reduction on gas-diffusion electrodes by distinctive hydrophilic-hydrophobic catalyst layers

Rabiee, Hesamoddin; Ge, Lei; Zhao, Jing; Zhang, Xueqin; Li, Mengran; Hu, Shihu; Smart, Simon; Rufford, Thomas E.; Zhu, Zhonghua; More Authors

**Important note**
To cite this publication, please use the final published version (if applicable).
Please check the document version above.

# Regulating the reaction zone of electrochemical $CO_2$ reduction on gas-diffusion electrodes by distinctive hydrophilic-hydrophobic catalyst layers

Hesamoddin Rabiee [a,b,c], Lei Ge [b,c,*], Jing Zhao [a], Xueqin Zhang [a], Mengran Li [c,d], Shihu Hu [a,**], Simon Smart [c,e], Thomas E. Rufford [c], Zhonghua Zhu [c], Hao Wang [b], Zhiguo Yuan [a]

[a] Australian Centre for Water and Environmental Biotechnology (ACWEB, formerly AWMC), The University of Queensland, St. Lucia, Queensland 4072, Australia
[b] Centre for Future Materials, University of Southern Queensland, Springfield Central, QLD 4300, Australia
[c] School of Chemical Engineering, The University of Queensland, Brisbane, QLD 4072, Australia
[d] Department of Chemical Engineering, Faculty of Applied Sciences, Delft University of 14 Technology, van der Maasweg 9, 2629Hz Delft, The Netherlands
[e] Dow Centre for Sustainable Engineering Innovation, School of Chemical Engineering, The University of Queensland, Brisbane, QLD 4072, Australia

## ARTICLE INFO

## ABSTRACT

Regulating the rational wettability on gas-diffusion electrodes (GDEs) plays a pivotal role to improve the efficiency of $CO_2$RR via fine-tuning the reaction zone and boosting the formation of triple-phase interfaces. Herein, we present a wettability regulation strategy that modulates the triple-phase reaction zone in the catalyst layer of GDEs. This strategy was employed on a flow-through hollow fiber GDE coated with a Bi-embedded catalyst layer. Compared to other ex-situ methods (e.g., adding wetting agents) affecting the bulk of electrocatalysts or catalyst layer, we create distinctive hydrophilic-hydrophobic regions within the catalyst layer. Catalyst layer with hydrophilic-hydrophobic regions outperforms the fully hydrophilic one by facilitating the species transport, boosting triple-phase interface formation, and maximizing the active sites. This regulation strategy showed stable wettability during $CO_2$RR cathodic conditions, evidenced by the direct measurement of penetration depth. The electrode with the regulated wettability exhibited over 80% catalyst utilization and 4 times higher formate partial current density (~150 mA cm$^{-2}$ with FE$_{formate}$> 90%) compared to the untreated electrode, outperforming other GDEs employed for $CO_2$RR to formate in the same concentrations of bicarbonate. The finding of this versatile microenvironment regulation strategy can be extended to GDEs used for other gas-phase reactions.

## 1. Introduction

Electrochemical $CO_2$ reduction reaction ($CO_2$RR) coupled with renewable electricity has attracted much attention for $CO_2$ conversion to chemicals/fuels at ambient conditions with a variety of products, depending on the electrocatalysts [1,2]. Therefore, it has been a race for more efficient electrocatalysts based on the desired reaction/product in the past decade [3–5]. In addition, gas-diffusion electrodes (GDEs) have been commonly employed in recent years to resolve the issue of sluggish $CO_2$ mass transport and low aqueous solubility [6]. GDEs directly deliver $CO_2$ in the vicinity of the catalyst, maximize $CO_2$ concentration, and shorten the diffusional pathway [7–11]. Despite the recent progress in GDE design/fabrication, conventional planar GDEs are fabricated

through complicated multi-steps and suffer from drawbacks such as flooding, thereby more advanced GDE structures are required [12].

Hollow fiber GDEs (HFGDEs) made of Cu were lately fabricated and promising results for $CO_2$RR were obtained, owing to their tubular shape, adjustable geometry (pore size, diameter, etc.), and high catalytic active area [13]. In addition, hollow fiber GDEs pass $CO_2$ through their internal side, therefore they do not require a separate chamber to deliver gas and can be versatilely mass-produced via facile dry-wet process, while planar GDEs are often fabricated via more complex multistep procedures as they consist of several layers. As Cu is a non-selective electrocatalyst for $CO_2$RR [14–16], the selectivity of Cu-based HFGDEs has been tuned via different methods, such as valence-controlled Sn deposition to produce formate [17], alloy Cu with the electrodeposited

---

* Corresponding author at: Centre for Future Materials, University of Southern Queensland, Springfield Central, QLD 4300, Australia.
** Corresponding author.
*E-mail addresses:* lei.ge@usq.edu.au (L. Ge), s.hu@awmc.uq.edu.au (S. Hu).

Sn (bronze HFGDEs) [18,19], or loading 2D Bi-based nanosheets to boost reactions sites [20]. However, proposing a general catalyst loading strategy effective for various reactions with the flexibility of loading the desired electrocatalysts for the target products of $CO_2RR$ remains a challenge. Unlike conventional flow-by GDEs, HFGDEs have a flow-through configuration, thereby $CO_2$ is forced through the hollow fiber pores, therefore $CO_2RR$ occurs on the outer side of HFGDEs, and products and unreacted $CO_2$ are in the electrolyte side. This diminishes the concentration gradient and leads to enhanced $CO_2$ supply to the catalyst layer, particularly at high catalyst loadings and current densities [21].

Besides the electrode structure, the wettability of the electrode plays a vital role to enhance the microenvironment of $CO_2RR$ and maximizing triple-phase interfaces as catalytic active sites [22]. The super hydrophilic electrode surface may lead to undesired wetting of the GDE, blockage of the gas delivery porous layer, and flooding [23]; while the superhydrophobic surface does not provide sufficient contact between the electrolyte and the electrocatalyst. As a result, the co-existence of hydrophilic-hydrophobic conditions is argued to be the optimal condition [24,25]. Methods such as plasma treatment on GDE [25], doping hydrophobic agent [24], or thermal treatment [26] on the electrocatalyst have been studied and promising results were achieved. But these methods target the bulk of GDE or electrocatalysts and affect the hydrophilicity of the whole catalyst layer, thus a strategy to precisely wet a certain depth of a GDE can provide a two-region hydrophilic-hydrophobic within the catalyst layer. In this scenario, the formation of triple interfaces is boosted, resulting in maximized catalyst utilization and high current densities. In addition, the unfavorable contact between the electrolyte and substrate can be limited, avoiding the pore flooding of GDEs and improving their long-term stability [27]. In tuning the local reaction environment, other parameters such as the local pH and $CO_2/H_2O$ ratio have also been shown to be effective, and recent studies have attempted to tune these parameters via treatment with ionomers [28,29] or polymer binders [30,31].

Herein we present a novel strategy to create distinctive wetting regions on a flow-through dual-layer HFGDE prepared via depositing a Bi-embedded carbon nanotubes (CNT-Bi) catalyst layer on Cu hollow fiber flow-through GDE for efficient $CO_2RR$ to formate. The wettability of dual-layer HFGDEs is regulated via in-situ electrochemical oxidation to control the depth of electrolyte penetration into the CNT layer and create a two-region hydrophilic-hydrophobic environment, as evidenced by confocal fluorescence images. The formation of enriched triple-phase interfaces along with having nanocatalysts, conductive CNT scaffold, and finer gas bubbles as $CO_2$ passes through the CNT layer, results in high current densities. Moreover, catalysts are in direct contact with CNT as the charge distributor without being covered and inactivated by an ionomer or a binder [32]. The dual-layer HFGDE with the optimal wettability exhibited approximately four times higher formate current density than that for the untreated electrode, outperforming other GDEs used in non-alkaline media with the same concentrations. The formation of hydrophilic-hydrophobic regions in the CNT layer and abundant microchannels to pass $CO_2$ leads to a tuned local microenvironment with enhanced triple-phase interfaces. The strategy presented in this study can be beneficial as a general approach for other products of $CO_2RR$ via loading CNTs with the desired electrocatalysts, or other gas-phase electrolysis systems.

## 2. Experimental

### 2.1. Fabrication of dual-layer hollow fibers

Firstly, copper hollow fibers were prepared by the phase inversion process, similar to our previous work [17]. The solution of 65 wt% copper particles (5–10 μm, 99%, Sandvik, UK), 8.75 wt% polymer (Polyethersulfone Ultrason 6020 P, BASF, Germany), and 26.25 wt% solvent (N-methyl-2-pyrrolidone) were extruded into a spinneret rig

(outer and inner diameters were 1.9 mm and 0.7 mm, respectively) to the non-solvent (water) bath. When the phase inversion between NMP and the non-solvent occurs, polymeric solution solidifies into a tubular shape (green hollow fibers) and is stored there for 24 h to completely remove the solvent. To make the green hollow fibers conductive, the polymer was removed at 600 °C in a tubular furnace (for 2 h in the air atmosphere). After that, the oxidized Cu hollow fibers were reduced back to Cu by hydrogenation in $H_2/Ar$ atmosphere (20%/80%) at 500 °C for 1 h. All chemicals were purchased from Sigma unless otherwise specified.

Bi-incorporated carbon nanotubes (CNT-Bi) were prepared via the chemical reduction method using $NaBH_4$ as the reducing agent [33]. Firstly, the solution of 4 ml of 0.25 mol $L^{-1}$ $Bi(NO_3)_3.5$ $H_2O$, 4 mmol trisodium citrate dehydrate, and including 0.1 ml of $HNO_3$ were added to 150 ml of DI water. Subsequently, 0.2 g CNT (multi-walled carbon nanotubes, OD: 10–20 nm, Length: 20–30 μm, ACS Material, USA) was added to the solution. After stirring for 30 min, 60 ml of $NaBH_4$ solution (0.1 M) was added drop-wise under vigorous stirring at room temperature. After 8 h, the black precipitate was filtered and washed several times by DI water and dried in a vacuum oven.

The CNT-Bi was subsequently deposited on the outer side of Cu HFGDE via electrophoretic deposition to fabricate dual-layer HFGDEs [34]. Briefly, 0.2 g CNT-Bi were dispersed in 100 ml water and 0.125 g of hexadecyltrimethylammonium bromide (CTAB) surfactant was added to the solution. The solution was sonicated via a probe sonicator for 30 min. One end of the Cu HFGDE was sealed by epoxy. The electrophoretic deposition was carried out using a DC power supply at 17.5 V at different durations (3, 5, 7, and 10 min), with a stainless-steel mesh in the positive port and Cu HFGDE in the negative port. The treated dual-layer HFGDEs were kept for 1 h in a diluted bicarbonate solution (0.01 M) solution to remove CTAB as the bicarbonate anion attaches to the cationic head of CTAB and remove it from CNTs surface. This was followed by keeping for another hour in DI water before letting them dry in the $N_2$ atmosphere.

### 2.2. Tuning the wettability of dual-layer HFGDEs

The wettability of the dual-layer HFGDEs was tuned via applying a certain anodic bias voltage for a controlled duration of time by a DC power supply (PLH250, Aim-TTi Instruments Ltd. UH)). The dual-layer HFGDE was connected to the positive side (anode) and a stainless-steel mesh was used as the cathode side. 0.5 M $KHCO_3$ (identical to the electrolyte used for $CO_2RR$) was used as the electrolyte during wettability treatment. The minimum voltage required to induce changes in the wettability was found via applying voltages from 0.5 to 3 V for 5 s and the changes in the contact angle were monitored to recognize the minimum voltage needed. Furthermore, the duration of the applied voltage was altered from 5 to 30 s to study its effects on the wettability and $CO_2RR$ performance of the dual-layer HFGDEs. The samples were stored in DI water for 30 min and dried in an $N_2$ atmosphere before performance analysis and characterizations.

### 2.3. Characterizations

A Hitachi HF5000 (accelerating voltage of 200 kV) was used to acquire transmission electron microscopy (TEM) images. A JOEL-7100 F (equipped with an energy dispersive X-ray analyzer (EDX)) was used to achieve field emission scanning microscopy (FESEM) images. X-ray diffraction (XRD) and X-ray photoelectron spectroscopy (XPS) were respectively obtained on a Rigaku SmartLab (Cu Kα (λ = 1.5405 Å) radiation source), and a Kratos Axis ULTRA XPS with a 165 mm hemispherical electron energy analyzer and a monochromatic Al Kα (1486.6 eV) radiation source at 15 kV (10 mA). XPS data were analyzed by CASA® software (calibrated to the C 1 s signal at 284.8 eV). Custom-made sessile drop equipment was used to measure the water contact angle at 25 °C by dropping 1 μl of DI water on the outer surface of the

electrodes. Thermogravimetric analysis (TGA) was conducted on a Perkin Elmer Instruments STA 6000 Thermo Gravimetric Analyser with a heating rate of 5 °C from 30 °C to 800 °C under Air. Confocal laser scanning microscopy was utilized to estimate the depth of electrolyte penetration into the CNT layer of dual-layer HFGDEs. The measurements were carried out on an LSM 510 Inverted META (Zeiss, Germany) confocal laser scanning microscopy. To conduct the analysis, 200 μl of sodium fluorescein (0.5 M) as the tracing dye was deposited into a confocal dish, and the dual-layer HFGDE was placed onto the liquid droplet. A confocal microscope with a × 40 (water) objective lens (LD Plan-Neofluar40x/0.6 Corr M27) coupled with a BP 505–550 filter was used with a 488-nm laser from the bottom side of the dish to the dual-layer HFGDE surface.

## 2.4. Calculation of $CO_2$ permeability through the HFGDEs

The permeability of the HFGDEs was calculated by measuring gas flux and pressure drop across the hollow fibers and using the following equation [17]:

$$P = \frac{F.L}{A\Delta p} \tag{1}$$

where, P is the gas permeability [$mol.m.m^{-2}.pa^{-1}.s^{-1}$], F is molar flow rate [$mol.s^{-1}$], L is the HFGDE's wall thickness [μm], A is the HFGDE's outer surface area [$m^2$], and $\Delta p$ is the pressure drop [pa] across the hollow fiber ($\Delta p$ is read from a pressure gauge installed on $CO_2$ line before the hollow fiber). P is reported in Barrer (1 Barrer = 3.35 × $10^{-16} \frac{mol.m}{m^2.pa.s}$).

## 2.5. Electrochemical reduction of $CO_2$ and product analysis

$CO_2$RR experiments were conducted in a 3-electrode H-cell. The cathode/anode compartments each had a volume of 200 ml, and 170 ml of catholyte/anolyte was used. Hollow fiber GDEs (4.5–5 cm, diameter of around 1.3 mm) were used as the working electrode (cathode). The counter electrode (anode) for the anodic water splitting was a Pt wire. An Ag/AgCl (3 M NaCl, Bioanalytical Systems, BASi, USA) as the reference electrode was placed near the working electrode. The electrolyte was 0.5 M $KHCO_3$. Nafion 117 Proton Exchange Membrane (Fuel Cell store) separated the cathode and anode chambers. The HFGDEs were sealed in one end with epoxy and $CO_2$ (99.9%, Coregas, Australia) was fed from the other end. Gas flow rate was set at 20 ml min$^{-1}$ by a mass flow controller (Bronkhorst, Netherlands, ± 1% resolution). The potentials in Ag/AgCl scale were converted to the reversible hydrogen electrode (RHE) scale via E (V vs. RHE) = E (V vs. Ag/AgCl) + $E^o_{Ag/AgCl}$ + 0.0591 pH, $E^o_{Ag/AgCl}$ is 0.209 for the Ag/AgCl reference electrode filled with 3 M NaCl solution. A Metrohm LL Unitrode PT1000 probe was used to measure the pH of the catholyte. A BioLogic SP-200 potentiostat was used to collect the data (e.g., linear scanning voltammetry (LSV), chronoamperometry, and cyclic voltammetry (CV)) [13,20]. The electrodes were conditioned by CV scans between − 1 and − 1.6 V vs. Ag/AgCl (100 mV s$^{-1}$) followed by 30 min pre-reduction at − 1.6 V vs. Ag/AgCl under $CO_2$ purging until a stable current was recorded [35]. The current densities (mA cm$^{-2}$) are reported based on the outer surface area of the tubular electrodes.

The dual-layer capacitance ($C_{dl}$) of HFGDEs was used to estimate the electrochemically active surface area of the electrodes and was obtained from CVs over a 0.1 V window near the open-circuit voltage at scan rates from 20 to 100 mV s$^{-1}$ via:

$$C_{dl} = J \left/ \left(\frac{dV}{dt}\right)\right. \tag{2}$$

where, C is the capacitance, J is the current density at the center of 0.1 V electrochemical window, and $\frac{dV}{dt}$ is the CV scan rate. CV scans to obtain

$C_{dl}$ were conducted while purging $CO_2$ through the HFGDEs.

LSVs, with the sweeping rate of 5 mV s$^{-1}$, and from − 0.1 V to − 1.3 V vs. RHE were obtained in $CO_2/N_2$-saturated media after half an hour of gas purging through hollow fiber electrodes and reaching pH steady state. The $CO_2/N_2$ flow (10 ml min$^{-1}$) continued during the test. Chronoamperometry was performed under $CO_2$ purging through the HFGDEs for 1 h at potentials between − 0.7 and − 1.2 V vs. RHE to obtain the faradaic efficiency (FE) of products (formate, CO, and $H_2$) at various potentials. Gas and liquid samplings were done after 30 min of applying potential and reaching the steady-state condition.

Formate generation was measured by a high-performance liquid chromatography (HPLC) (Shimadzu, Hi-Plex H, 7.7 × 300 mm, 8 μm column, SPD-20A/20AV UV-Vis detector). Formate was the only liquid product detected by HPLC. The FE$_{formate}$ was calculated using the following equation:

$$FE_{formate} = \frac{2Fn_{formate}}{Q} \tag{3}$$

where, F is Faraday's constant (96485 C.mol$^{-1}$), n$_{formate}$ is the moles of the produced formate, from HPLC. Q is the total charge during the experiment (calculated by the measured current and sampling time).

Gaseous products (CO and $H_2$) were analyzed with a Shimadzu 2014 GC, equipped with a ShinCarbon packed column (ST 80/100, 2 mm ID, 1/8 OD Silico, Restek). $H_2$ was detected by a thermal conductivity detector (TCD)and the rest of the gases were detected on a flame ionization detector (FID). The FE of gaseous products were determined via the following equation:

$$FE_i = \frac{e_i \times F \times P \times V \times X_i}{J \times R \times T} \times 100 \tag{4}$$

where, $e_i$ is the electron transfer required to produce one mole of a gaseous product ($e_i$ is 2 for $H_2$ and CO), $X_i$ is the concentration of the products in the reactor gas outlet flow measured by GC, V is the effluent gas volumetric flow rate, measured by a digital flow meter, P is the atmospheric pressure (101.3 kPa), and J is the current (mA) obtained from the potentiostat.

The stability test (for 24 h) was examined in a home-built flow-cell (Fig. S1) by peristaltic pumps to circulate electrolytes (0.5 M $KHCO_3$) in the anodic and cathodic sections. Anode and cathode compartments had a volume of 20 ml and two extra reservoir containers with a volume of 2 L were used for catholyte and anolyte circulation with a flow of 10 ml min$^{-1}$, and $CO_2$ purging through the electrodes (20 ml min$^{-1}$). The desired number of HFGDEs can be employed in the flow-cell reactor, and as seen in Fig. S1, two HFGDEs are used. To separate gas (including unreacted $CO_2$ and gas products) from the electrolyte, the outlet of the flow reactor was connected to a water trap bottle. Samplings for liquid and gas were done once per hour. For each electrochemical test, the average of three times repeat is reported.

## 3. Results and discussion

### 3.1. Characterization/fabrication of dual-layer HFGDEs

Dual-layer HFGDEs were designed and fabricated on Cu hollow fiber substrate followed by electrophoretic deposition of a thin layer of CNT-Bi and regulating its wettability via electro-oxidation to be used as a flow-through GDE to deliver $CO_2$ through inside of the hollow fiber, as schematically shown in Fig. 1a. Hollow fiber GDEs were prepared via the dry-wet process showed a uniform structure with a consistent wall thickness of around 150 μm (Fig. S2a). The metallic HFGDEs showed high electrical conductivity (Table S1), resulting from complete removal of polymeric binder as confirmed in EDX analysis (Fig. S3), and well-connected Cu particles (Fig. S2b) after sintering at a high temperature. The hollow fibers showed structural flexibility to be slightly bent (Fig. S4) and can be hand-held as shown in Fig. 1b.
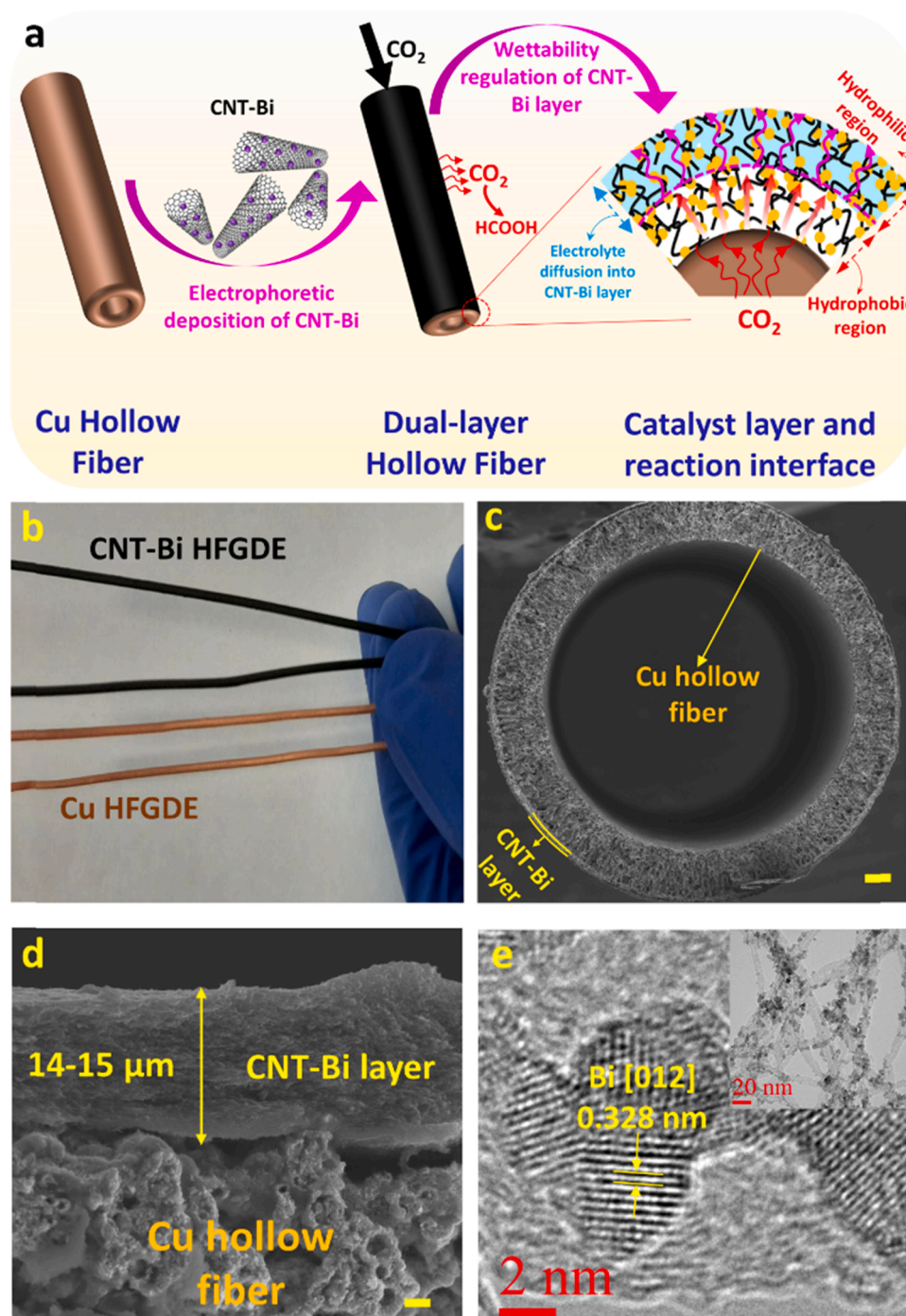
**Fig. 1.** a) Schematic of dual-layer HFGDE fabrication with CO$_2$RR occurring on the CNT-Bi layer and CO$_2$ is purged through the internal side. Wettability regulation results in distinctive hydrophilic-hydrophobic regions and having triple-phase-rich interfaces; b) Hand-held Cu and dual-layer HFGDEs; c, d) Cross-sectional FESEM images of dual-layer HFGDE prepared with 10 min of electrophoretic deposition. (Scale bar: c: 100 μm, d: 2 μm); e) TEM and HRTEM of Bi-imbedded CNTs.

The dual-layer HFGDEs are made by deposition of a uniform layer of CNT-Bi on the outer side of Cu HFGDE (Fig. 1c and d) via the electrophoretic deposition method. Firstly, bismuth particles were uniformly attached on CNTs via NaBH$_4$-assisted chemical reduction method (Fig. S6) with a particle size of around 5–10 nm as seen in TEM images (Fig. 1e, S6), with the loading value of approximately 53 wt%, estimated from TGA analysis (Fig. S7). XPS spectrum of CNT-Bi showed peaks with a binding energy of around 155–163 eV (Fig. S8a). The two character-istic peaks of Bi 4f (Fig. S8b) are related to the Bi-oxide caused by the Bi surface oxidation due to air exposure [20]. XRD analysis confirmed the presence of bismuth on CNTs with peaks at 27.1°, 37.9°, and 39.6°

attributed to Bi [012], [104], and [110] crystalline planes, respectively (Fig. S8c). The lattice space observed in HRTEM (Fig. 1e) was also consistent with the crystalline peaks in the XRD spectra.

To coat CNT-Bi via electrophoretic deposition technique, CTAB as a surfactant with the cationic hydrophilic head was used to positively charge CNT-Bi (Fig. S9). Therefore, CNT-Bi is driven toward Cu HFGDE (Fig. S10), resulting in the deposition of a uniform CNT-Bi layer [36]. Later on, CTAB is fully removed by immersing the HFGDE in a diluted bicarbonate solution (0.01 M). The high-resolution SEM images revealed the tight thread among the CNTs and close contact between the Cu substrate and CNT layer (Fig. S11). The thickness of the CNT layer

can be controlled via altering the deposition duration (Fig. S12). A 10 min deposition duration led to having a thickness of around 14–15 μm (Fig. 1d), which is the usual catalyst layer thickness with the common planar GDEs [7]. The surface of the dual-layer HFGDEs was homogenously covered by CNTs (Fig. S12), leading to having visibly

smaller surface pore size as compared with Cu HFGDE (Fig. S13) therefore finer $CO_2$ bubbles on the HFGDE surface. The regulation of surface pores led to the homogenous distribution of $CO_2$ gas while passing the CNT layer. It was observed that the CNT layer did not cause any substantial pressure resistance due to the highly porous structure
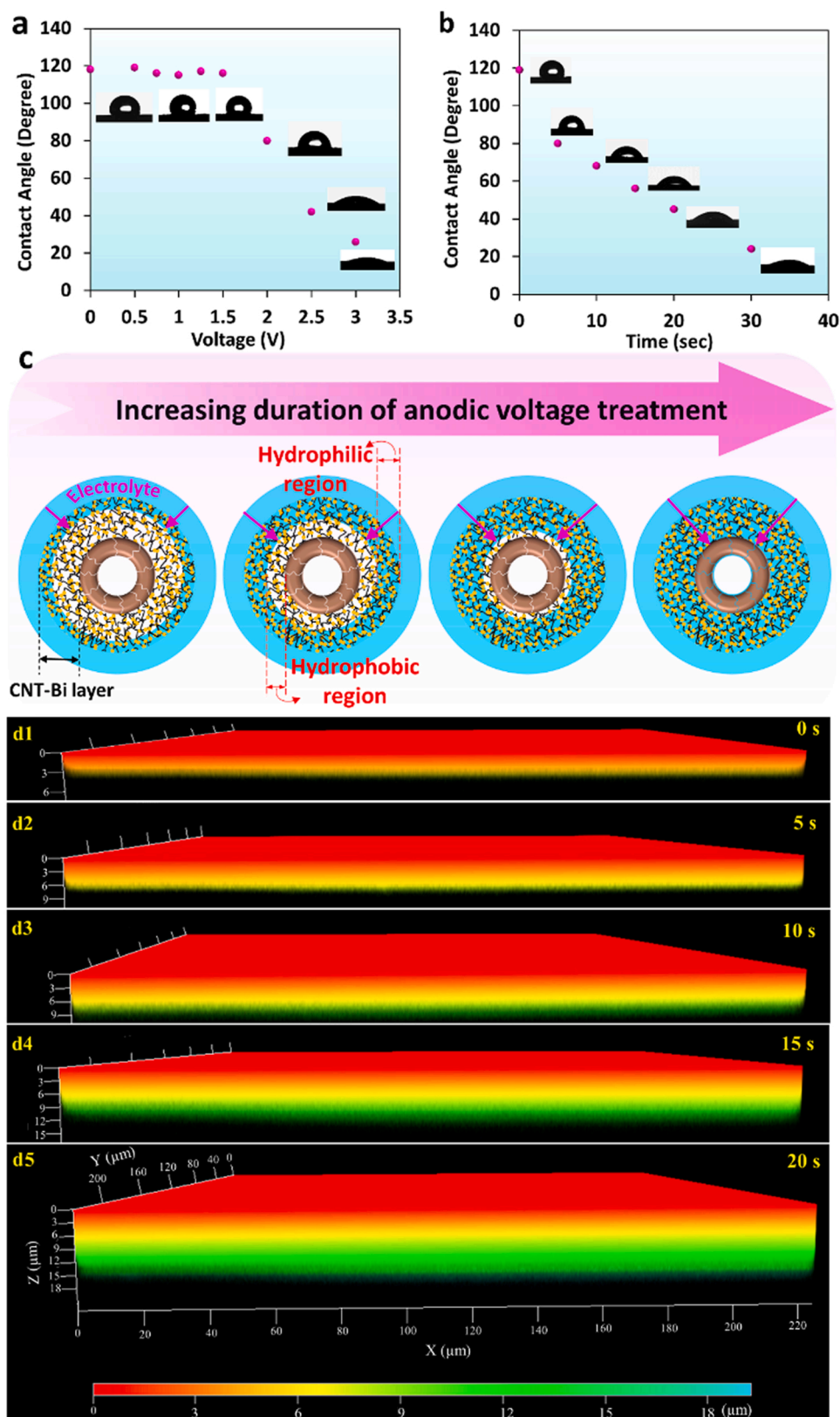


**Fig. 2.** a) Contact angle of dual-layer HFGDE after 10 s wettability regulation via anodic voltage at various voltage values; b) The effect of duration of anodic voltage treatment at 2.0 V; c) Schematic of progressive wettability changes on the CNT layer of dual-layer HFGDE and formation of hydrophilic-hydrophobic regions; d1-d5) Cross-sectional fluorescence confocal laser microscopy indicating the depth electrolyte penetration into the CNT layer for dual-layer HFGDEs treated with 2.0 V anodic voltage at different durations. (Z represents the penetration depth into the CNT layer, Z = 0 is the outer surface of dual-layer HFGDE).

and with a pressure drop of 0.6–0.8 atm, the $CO_2$ flow reached 20 ml min$^{-1}$. The permeability of the dual-layer HFGDEs was around $4.1 \pm 0.5 \times 10^{+6}$ Barrer, calculating via Eq. (1).

### 3.2. Creation of dual-wetting regime in HFGDEs

The CNT-coated (dual-layer) HFGDE had an apparent contact angle of 118, showing the intrinsic hydrophobicity of the electrode surface. For the dual-layer Bi-CNT on Cu HFGDE, the Bi-CNT layer acts as the catalyst layer, therefore the maximum contact between the electrolyte and the catalyst-embedded CNT layer results in an enhanced interface for the electrolyte-electrocatalyst. For this matter, having a tuned hydrophilic surface leads to the penetration of electrolyte into the CNT layer, wetting the electrocatalyst, thus increasing the catalyst utilization [25]. Meantime, having a hydrophobic layer to impede the contact between the electrolyte and the substrate is necessary to avoid non-selective reactions on the substrate (Cu is non-selective for $CO_2RR$). Therefore, an in-situ method to control the depth of electrolyte penetration into the CNT layer and create a hydrophilic-hydrophobic region has advantages over other methods where the bulk catalyst is treated beforehand without creating two regions with different wettability features. We suggest that a precise time-dependent electro-oxidation of the CNT layer by a bias voltage increases the surface wettability. To study the applicability of this method, three questions should be answered: 1. What bias voltage is sufficient for this regulation method? 2. How long oxidation is required for the desired hydrophilicity? and 3. Is this hydrophilicity regulation strategy irreversible and stable under cathodic conditions?

To find the threshold of bias voltage, contract angles of the electrodes were recorded after applying 5 s of various oxidative bias voltages. During the wettability regulation with the anodic voltage, CNTs are oxidized [37] and this stands as the main reason for changes in wettability and decrease of contact angle of dual-layer HFGDEs. Wang et al. showed that the binding energy of water with oxidized CNT is much higher than that with pristine CNT [38]. This indicates that water interaction with oxygen adsorbed CNT surface is substantially higher than the CNT before electro-oxidation which makes the CNTs hydrophilic. When CNT oxidation occurs, the oxidized part is wetted by the electrolyte, and in this way, the two-region can be obtained. It was seen that the minimum voltage required to trigger changes in the contact angle was 2 V, which correlates well with the minimum anodic voltage of 1.7–1.8 V for CNT oxidation on the literature [38], while a lower bias voltage didn't result in any significant change (Fig. 2a). The water contact angle decreased from 119° to nearly 79° after 5 s of applying 2 V. Expectedly, a higher voltage led to a larger drop in the contact angle. Herein, it was attempted to find and apply the lowest possible voltage (threshold) to minimize any probable damaging effects of the oxidation on the Cu substrate. In addition, changes in the water contact angle are more abrupt at higher voltages, due to the faster oxidation, thereby working with the minimum voltage makes it feasible to effectively fine-tune the hydrophilicity.

In addition to the voltage, the duration of applying voltage can influence the wettability of the electrodes' surface. A voltage of 2 V was applied from 5 to 30 s to probe changes in the water contact angle and a more hydrophilic surface was achieved by increasing the duration of anodic voltage. The gradual- decrease in the water contact angle (hydrophobic to the hydrophilic surface) can be seen in Fig. 2b. It can be speculated that during the surface treatment with the bias voltage, oxidation occurs from the outer side of the CNT layer which is in touch with the electrolyte. Therefore, with longer voltage applied, the deeper layer of the CNT layer is progressively oxidized, and the electrolyte slowly sinks into the depth of the CNT layer, resulting in extension of wettability changes to the inner of the CNT layer. This is schematically illustrated in Fig. 2c. Using this method, the electrolyte can be confined within the desired depth of the CNT layer due to the creation of separated hydrophilic and hydrophobic areas. While a longer voltage

treatment leads to complete wetting of Cu substrate and possibly diffusion of electrolyte into the pores. The surface oxygen content of the HFGDEs from XPS analysis also showed an increasing trend with extending oxidation duration (Fig. S14a), indicating the formation of oxygen-containing groups such as hydroxyl and carboxyl groups. This increase of oxygen-containing functional groups is consistent with the decreased water contact angle on the electrodes, as seen in Fig. 2b. Formation of C-O and C=O functional groups was also observed in the analysis of the C1s XPS peak of the CNT-Bi 15 s electrode (Fig. S14b). The main peak at around 285 eV is related to graphitic carbon, while after the electro-oxidation treatment, oxidized carbon species were detected at peaks between 286 and 289 eV [39]. The post-$CO_2RR$ Bi 4f XPS spectra showed the existence of both $Bi^0$ and $Bi^{3+}$ species (Fig. S14c). This indicates that $Bi^{3+}$ from electro-oxidation treatment and/or air exposure is partially reduced to $Bi^0$, therefore both $Bi/Bi^{3+}$ species are present during $CO_2RR$ [40].

Furthermore, the depth of the electrolyte in the CNT layer should be correlated with the duration of wettability regulation to find the optimal conditions. The confocal laser microscopy images of the dual-layer HFGDEs treated at various durations of anodic voltage gave us direct evidence regarding the depth of electrolyte penetration into the CNT layer. As can be seen in Fig. 2 d1–d5, the trace liquid diffuses around 3 μm into the CNT layer of the dual-layer HFGDE before wettability regulation (Fig. 2 d1). The penetration depth increased with the duration of voltage treatment and after 15 s of, the penetration depth of around 10–11 μm was observed (Fig. 2 d4), and for 20 s, the penetration is $\geq$ 15 μm. Considering the thickness of the CNT layer (14–15 μm, Fig. 1d), it can be said that after 15 s of wettability regulation, the optimal electrolyte penetration while having a hydrophilic-hydrophobic region can be obtained. In addition, the confocal images show a smooth and uniform depth profile, confirming the homogeneity of the increase in penetration depth of the dual-layer HFGDEs.

The electrodes with tuned wettability should be able to keep the hydrophobic-hydrophilic regions under cathodic conditions. This ensures that during $CO_2RR$, the electrolyte is confined within the desired depth of the catalyst layer. To examine the stability of this wettability regulation method under cathodic reactions, the depth liquid penetration into the CNT layer of the electrode was measured before and after 24 h at − 1.0 V vs. RHE while $CO_2$ purging. The measurements showed no substantial changes in the penetration depth (Fig. S15), indicating that the oxidation of CNT is irreversible [38] and the CNT layer could retain its tuned wettability under cathodic conditions [38]. Similarly, the contact angle measurements before and after reduction reaction showed no significant drop (Fig. S15), consistent with the results of confocal microscopy. It was also observed that the C-O functional groups created on CNTs after the wettability regulation were still present after reduction reactions, confirming that these functional groups and the defects on the CNT surface are not reversible under cathodic conditions of $CO_2RR$. This method of triple-phase interface control makes it possible to effectively control the depth electrolyte penetration into the CL as it happens via progressive oxidation from the top layer. Unlike methods such as thermal oxidation of the catalyst [26], chemical functionalization [41], or plasma treatment [25] which are done externally on the GDE bulk, in this method wettability enhancement can be precisely controlled in the desired depth to provide two regions with different hydrophilicity behavior.

### 3.3. $CO_2RR$ performance

The $CO_2RR$ performance of the HFGDEs was studied to determine the effects of wettability regime regulation on the reaction rate and product selectivity. The configuration of gas delivery on HFGDEs is flow-through, therefore $CO_2$ is pushed through the hollow fiber porous walls by a pressure gradient (0.6–0.8 bar in this study) which should be higher than the capillary pressure to push $CO_2$ into the CNT-Bi catalyst layer and the reaction happens on the outer surface (as seen in the

graphical abstract). In flow-by design from literature, the pressure gradient is usually zero because the carbon-based supports do not cause any gas transport resistance and $CO_2$ easily passes through the support and contacts the catalyst in the interface with electrolyte. Although, some studies have attempted to apply a pressure gradient over zero in flow-by design to control excessive penetration of the electrolyte into the GDE and hinder flooding [42]. Flow-through and flow-by configurations also differ where gas/liquid products and/or unreacted $CO_2$ are collected. With the typical flow-by cells, $CO_2$ diffuses through the planar GDE, and unreacted $CO_2$ and/or gaseous products are collected at the same feed side. However, in flow-through, as $CO_2$ goes through the catalyst layer, it increases $CO_2$ supply rate and diminishes the $CO_2$ concentration gradient, and both liquid and gaseous reactants are collected at the same side. Therefore, having an optimal catalyst-electrolyte contact from a dual-wetting zone boosts the creation

of triple-phase interfaces within the catalyst layer. It was reported by Kas et al. that the $CO_2RR$ performance (current density and FE of CO) depended on the flow rate of $CO_2$ flow rate through the Cu hollow fiber when the flow rate was below 20 ml/min, but remained steady at higher flow rates, indicating that most active sites were involved in $CO_2RR$ at a high flow rate [13]. To allow us to compare our performance with other studies, including our previous ones [17,20], we accordingly chose a flow of 20 ml/min to ensure that the reaction was not limited by the lack of $CO_2$ supply.

LSV curves of the HFGDEs at a scan rate of 5 mV s$^{-1}$ were achieved and all the HFGDEs showed a similar trend with nearly zero reduction current densities at potentials more positive than $-0.1$ V vs. RHE (Fig. 3a). At more negative potentials, where $CO_2RR$ competes with hydrogen evolution, the current densities significantly increased and showed an intimate relationship with the wettability treatment
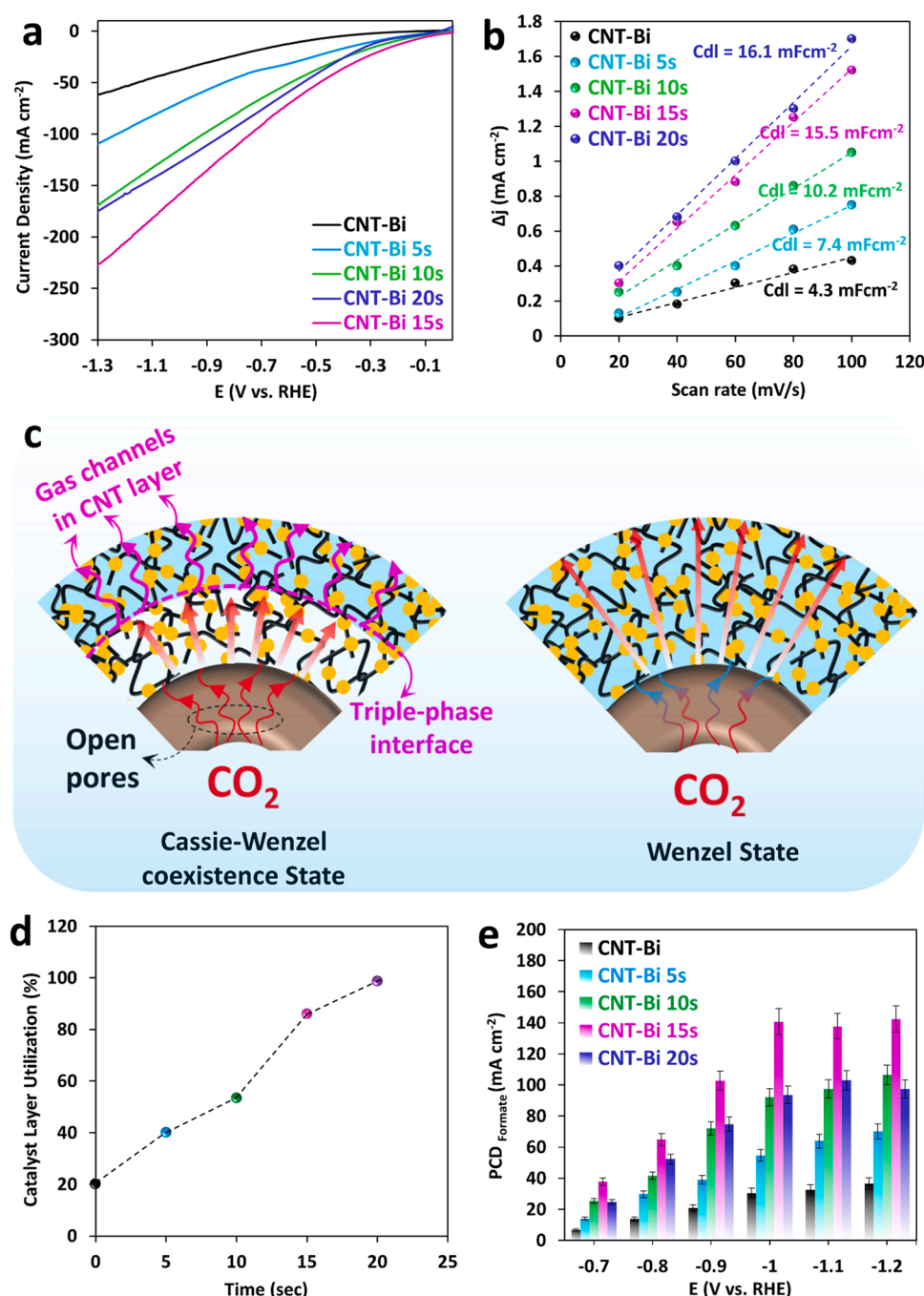


**Fig. 3.** a) Linear sweep voltammetry of hollow fiber electrodes while $CO_2$ supplied through HFGDEs; b) Dual-layer capacitance ($C_{dl}$) of electrodes; c) Schematic of triple-phase interface formation: left side refers to the coexistence of Cassie-Wenzel state and triple-phase interface is formed; right side refers to Wenzel state where electrolyte wets the CNT layer may lead to pore blockage; d) the ratio of catalyst layer utilization as a function of electrooxidation duration; e) Formate partial current density of dual-layer HFGDEs as a function of applied potential.

duration. The difference of LSV curves in $CO_2$- and $N_2$-purged electrolytes also showed the high activity of dual-layer HFGDEs for $CO_2$RR (Fig. S17a). For the untreated hydrophobic electrode, the lack of the proper solid-liquid interface between the $CO_2$-saturated electrolyte and the electrocatalyst leads to a lower current density. While higher current densities were observed for the HFGDEs with tuned wettability. This is consistent with the speculation of progressive extension of the reaction zone due to the deeper electrolyte penetration into the CNT layer, as confirmed in the confocal images (Fig. 2 d1–5) [43]. Among all the treated HFGDEs, the optimal current density was observed for the one after 15 s of wettability regulation. While for > 15 s, the hydrophilic area extends to the very end of the CNT layer, and a hydrophilic-hydrophobic region is not formed, resulting in fewer triple-phase interfaces [24]. The higher current density for HFGDE with 15 s of wettability regulation, despite the identical catalyst loading for all dual-layer HFGDEs, confirms the higher catalyst utilization when the solid-electrolyte interface is tuned.

Consistent with the current density trend, the analysis of electrochemical surface area (ECSA) also confirmed the improved contact between the CNT layer and the electrolyte and increase in the catalytic active area of the dual-layer HFGDEs with the tuned wettability. The dual-layer capacitance of the HFGDEs ($C_{dl}$) obtained from the CV cycles at various scan rates (Fig. S18), showed an increase with the duration of voltage treatment and depth of electrolyte penetration into the CNT layer (Fig. 3b). The increase in $C_{dl}$ is greater for the HFGDEs with up to 15 s of wettability regulation, the HFGDE with CNT-Bi 20 s showed a slightly higher $C_{dl}$, compatible with the depth of electrolyte penetration into the CNT layer. In addition, during the wettability regulation via electro-oxidation, abundant defect sites are created on the CNTs [39], which are known to improve CNTs hydrophilicity and increase the catalytic active surface area and the current density. The presence of CNTs as an effective conductive scaffold, holding nano-size catalysts, contributes to enhancing capacitance, electron/charge transfer, and catalyst utilization within the catalyst layer [33].
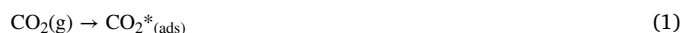
The regulation of surface wettability favors the formation of triple-phase interfaces within the CNT layer, schematically illustrated in Fig. 3c. Containing the electrolyte in a certain depth of the catalyst layer works in two ways: 1. Wetting the catalyst layer scaffold with the electrolyte and maximizing the catalyst utilization 2. Keeping the gas transportation channels open in the catalyst layer for efficient $CO_2$ delivery and saturating the electrolyte in contact with the electrocatalyst. Having a hydrophobic section in the CNT layer acts as the $CO_2$ distributor and leads to the formation of microchannels in the wetted region of the CNT layer. This is the optimal case as these microchannels create an abundant surface area for triple-phase formation. It should be noted that the microchannels within the CNT layer are assumedly continuing with the pores of the Cu HFGDE substrate, therefore the dual-layer HFGDE surface is not all gas pathways and the electrolyte penetrates the CNT layer while $CO_2$ is purging. In addition, it has been reported that wettability depends on the material properties, therefore the hydrophilic region can still become wet when in contact with the electrolyte, no matter how large the gas flow rate is [44]. In wettability studying, this is called Cassie-Wenzel coexistence (Fig. 3c, left), where the surface is neither super hydrophilic nor superhydrophobic [44] and is argued to be the optimal wettability status during $CO_2$RR [25]. While in the Wenzel state (Fig. 3c, right), the surface is fully wetted by the electrolyte. With the Wenzel state (electro-oxidation durations >15 s), it is expected that electrolyte gets in touch with the substrate pores, leading to pore blockage, disrupting uniform $CO_2$ delivery into the CNT layer and lowering the chance of triple-phase formation resulting in a lower current density. Therefore, the wetted area within the CNT-Bi layer where the catalyst is in contact with $CO_2$-saturated electrolyte, and areas of triple-phase interface formation (the interface of the hydrophobic-hydrophilic regions and the gas channels within the CNT-Bi layer (Fig. 3c, left)), are both the catalytic active sites in dual-layer HFGDEs.

Calculation of catalyst utilization ratio based on the wetting volume of CNT layer (details in the Methods section) also showed a substantial increase with duration of wettability regulation consistent with the trend observed for current densities. As can be seen in Fig. 3d, the untreated HFGDE showed poor catalyst utilization due to the poor catalyst-electrolyte contact, while it increased to over 80% for CNT-Bi 15 d HFGDE. The catalyst utilization ratio is based on the depth of electrolyte diffusion into the CNT-Bi layer and wetted area, although even within the wetted area there might be inactive sites due to gas trapping, etc., therefore the catalyst utilization is mainly for comparison.

We further studied the effects of wettability on the $CO_2$RR product selectivity of the dual-layer HFGDEs via the chronoamperometry analysis (Fig. S19). The highest FE of formate was obtained at − 0.9 to − 1.1 V vs. RHE (Fig. S16b), which is the common potential window of high formate selectivity on Bi-based electrocatalysts [40,45]. Formate FE of around 90% was obtained CNT-Bi 15 s HFGDE. The FE of CO was below 5% for all samples, except CNT-Bi 20 s HFGDE which showed higher $FE_{CO}$ due to the contact between the electrolyte and Cu substrate (Fig. S17c). The FE of $H_2$ drops significantly with the increase of the overpotential (Fig. S17d) which is related to the intrinsic characteristics of Bi-based materials to inhibit $H_2$ evolution [46]. At potentials more negative than − 0.9 V vs. RHE where the rate of $CO_2$ conversion is faster, the existence of gas microchannels and triple-phase interfaces provide sufficient $CO_2$ supply, which is the reason for a higher FE of formate observed on CNT-Bi 15 s dual-layer HFGDE. However, the highest formate partial current density (PCD) was achieved for the CNT-Bi 15 s HFGDE (Fig. 3e), owing to its highest current density and abundant triple-phase interface formation, which supplies sufficient $CO_2$ into the reaction zones, and its high catalyst utilization. For the case of pristine Cu HFGDE, FE of formate as high as 30% was observed at − 1.0 V vs. RHE, moreover, the formation of hydrocarbons ($CH_4$ and $C_2H_4$) was also observed on Cu HFGDE due to the non-selective nature of Cu electrocatalyst (Fig. S17e). However, since the Cu substrate cannot contact the electrolyte due to the controlled penetration of the electrolyte (confirmed by confocal microscopy in Fig. 2d), it does not interfere with the $CO_2$RR selectivity of the dual-layer HFGDEs.

The higher current density of CNT-Bi 15 s sample in GDE mode ($CO_2$ delivered through the HFGDE) compared to non-GDE mode ($CO_2$ is sparged in the electrolyte) (Fig. S17f), supports the role of triple-phase formation on the catalyst layer of HFGDE when $CO_2$ diffuses through the HFGDE wall towards the catalyst in GDE-mode [18]. The lower formate selectivity of the CNT-Bi 20 s HFGDE can be attributed to contact between the electrolyte and non-selective Cu, as seen in Fig. 2d5, which adversely affects the product selectivity (Figs. S17a, b, c). In addition, the lower chance for triple-phase formation on CNT-Bi 20 s HFGDE (Fig. 3c) leads to an insufficient $CO_2$ supply for the electrocatalysts, diminishing the catalytic activity with the CNT layer.

Altering the electrodes' wettability may also affect the kinetic of $CO_2$RR, as observed from the Tafel analysis. $CO_2$ electrolysis to formate is commonly accepted to start from $CO_2$ adsorption on the electrocatalyst surface, followed by multiple electron transfer and protonation steps as below:

$$CO_2(g) \rightarrow CO_2*_{(ads)} \tag{1}$$

$$CO_2*_{(ads)} + e^- \rightarrow CO_2*^-_{(ads)} \tag{2}$$

$$CO_2*^-_{(ads)} + H^+ \rightarrow *OCHO_{(ads)} \tag{3}$$

$$*OCHO_{(ads)} + e^- \rightarrow HCOO*^-_{(ads)} \tag{4}$$

$$HCOO*^-_{(ads)} + e^- \rightarrow HCOO^-_{aq} \tag{5}$$

Following $CO_2$ adsorption (step 1), electron transfer to form $CO_2*^-_{(ads)}$ (step 2), and protonation to form *OCHO (step 3), $HCOO*^-_{(ads)}$ is generated in step 4 and becomes liquid formate after the third electron transfer (step 5). Meanwhile, $CO_2$ electrolysis is competing with hydrogen evolution reaction ($2 H^+ + 2e^- \rightarrow H_2$). A lower Tafel slope is

indicative of a faster reaction and as can be found in Fig. 4a the lowest slope was observed for the HFGDE with 15 s of wettability regulation. This is due to the formation of an abundant triple-phase interface (as shown in Fig. 3b) which made the mass transport of $CO_2$ no longer the rate-limiting process. The increase in the active sites can also lead to the adjustment of reaction mechanism and rate-determining step during $CO_2RR$ [47]. Meanwhile, the Tafel slope of all electrodes was over 118 mV dec$^{-1}$, which is the reported Tafel slope if the rate-limiting step of $CO_2RR$ is one electron and $CO_2$ to form $CO_2$ *$_{(ads)}$ intermediate [48]. Thereby, adsorption binding of $CO_2$*$_{(ads)}$ intermediate can affect the reaction for the couple of $CO_2/CO_2$*$_{(ads)}$ [24].

The substantial increase in the reaction sites within the created triple-phase interfaces may alter the adsorption of intermediates (e.g., $CO_2$ *$_{(ads)}$), leading to changes in the reaction pathway. To confirm this speculation, adsorption/desorption of OH$^-$ as a surrogate for $CO_2$*$_{(ads)}$ was examined via conducting an LSV analysis in 0.1 M NaOH ($N_2$-purged). This has been commonly considered in several studies on $CO_2RR$ working with different electrocatalysts such as Ag, Bi, $Bi_2O_3$, Sn, $SnO_2$, and Cu [24,49–56]. During the oxidative LSV, the potential required for hydroxyl adsorption (the peak) was monitored and the lowest potential was seen for the HFGDEs without the wettability treatment (Fig. 4b). This indicates the highest binding energy (or strongest binding) for the untreated HFGDE [49]. This peak shifts to more positive potentials for the treated samples, indicating a weaker binding between the reaction sites and intermediates [50]. The weak binding towards the intermediates is beneficial for enhanced formate formation. $CO_2$ *$_{(ads)}$ adsorption on the reaction sites is the initial step of $CO_2RR$ to formate, and a strong surface stabilization of $CO_2$*$_{(ads)}$ leads to more barrier and hindered reduction/protonation of $CO_2$*$_{(ads)}$. Therefore, on the reaction sites of the electrode with the weakest $CO_2$*$_{(ads)}$ adsorption, the C atom in $CO_2$*$_{(ads)}$ will be more available for hydrogenation and facilitated formate formation [24]. Regulating the wettability of the electrode surface can lead to tuning the binding energy of the intermediates and enhance $CO_2RR$ performance. This observation is consistent with recent studies where the effect of catalyst pore structure, size, hydrophilicity/hydrophobicity (formation of triple-phase interfaces) on the binding energy of intermediate was explored and lower binding energy resulted in higher FE of formate [24,49,50].

### 3.4. Performance comparison and stability of dual-layer HFGDEs

Looking towards more practical conditions, we further tested the optimal dual-layer HFGDE (CNT-Bi 15 s HFGDE) for 24 h stability test in a purpose-built flow-type cell (Fig. S1). As can As can be seen in Fig. 4c, the dual-layer HFGDE showed a stable performance in terms of current density and FE of formate, with a negligible drop. Since the electrolysis in an H-cell is subject to bicarbonate/ion concentration polarization in the proximity of the electrode, and mass transport resistance, a higher current density was achieved in the flow cell. It was previously noticed that the CNT layer was able to retain its wettability level after going under cathodic conditions (Figs. S15 and S16), which is in accordance with the fairly stable performance seen in Fig. 4c. In addition, it is speculated that the wettability regulation is mainly governed by CNTs, and as oxidized carbon species were present on the CNTs after $CO_2RR$ (Fig. S14b), the CNT layer is able to maintain its wettability. Further, the flow-through configuration used here might contribute to facilitating product transportation out of the CNT-Bi catalyst layer and provide local pH stability. It was also seen that the structure of the dual-layer HFGDEs did not change, and the SEM images showed no substantial deformation (Fig. S20), indicating the stability of dual-layer HFGDEs during electrolysis. The promising stable performance of dual-layer HFGDEs in a flow-cell exhibits the potential of this electrode configuration for simplified electrolyzer designs since using HFGDEs eliminates the need for a separate chamber for $CO_2$ delivery (Fig. S1). We further compared the $CO_2RR$ efficiency achieved in this study with other Bi-based studies for formate production (Fig. 4d). Considering the current density and FE of formate, the efficiency seen in this study outperformed other Bi-based electrodes tested in neutral electrolytes (considering the electrolyte
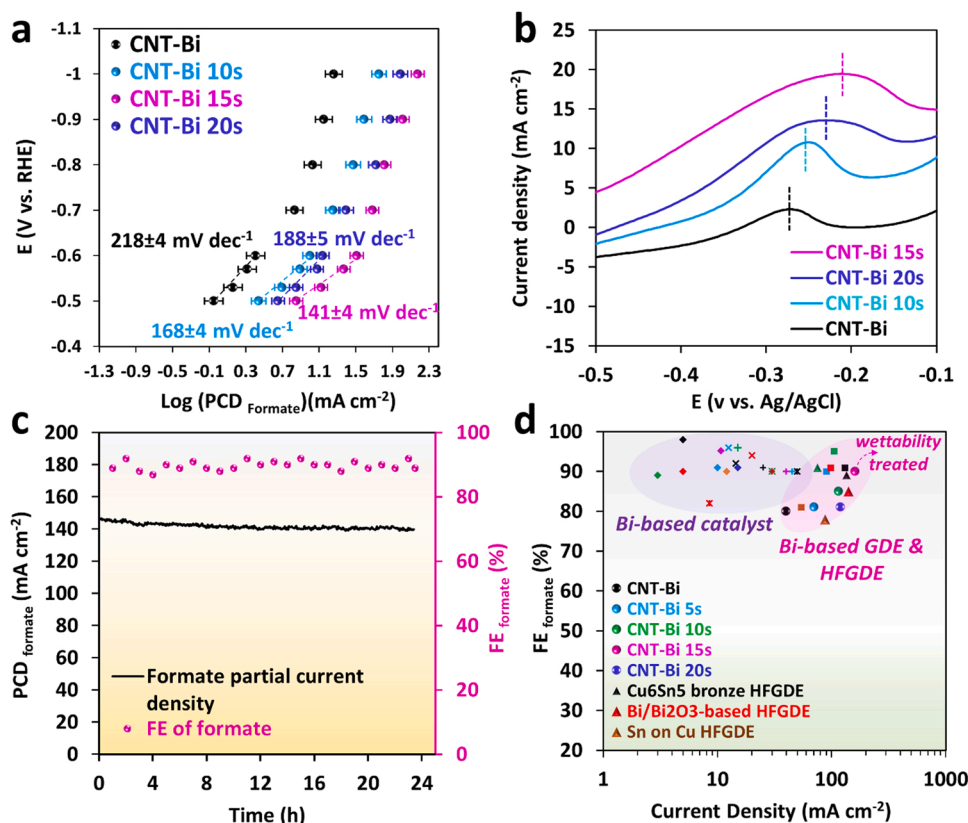


**Fig. 4.** a) Tafel plots of formate for dual-layer HFGDEs; b) Single oxidative LSV scans at 50 mV s$^{-1}$ in $N_2$-saturated 0.1 M; c) 24 h stability test at − 1.0 V vs. RHE: faradaic efficiency and formate partial current density in the flow reactor with CNT-Bi 15 s dual-layer HFGDE; d) $CO_2RR$ performance comparison of dual-layer HFGDEs with other Bi-based catalysts and GDEs/HFGDEs for formate production in neutral (bicarbonate) electrolytes with the same concentration (more details on $CO_2RR$ performance and electrolyte type in Table S2).

concentration), including our previous work on HFGDEs coated with 2D Bi/Bi-oxide nanosheets [20]. This confirms the potential of wettability-tuned dual-layer HFGDEs as an advanced electrode design for flow-through gas-phase electrolysis.

This strategy of wettability regulation can be effectively used for planar shape GDEs. CNTs or carbon black have been extensively used as the catalyst support, followed by a catalyst ink deposition to fabricate GDEs [33,57]. Applying a certain anodic voltage for a controlled duration after the catalyst deposition can control the hydrophilicity of the GDE surface and the depth of electrolyte penetration can be tailored. Especially, planar gas-diffusion electrodes with carbon-based gas-diffusion layers are run via flow-by configuration and are prone to flooding [23], therefore containing the electrolyte in the desired depth can circumvent flooding. In addition, dual-layer HFGDEs can be employed for other products of $CO_2RR$ or other gas-phase electrolysis reactions. CNTs can be loaded with the desired electrocatalysts, for example, Sn or Ag for $CO_2RR$ to CO production [58], Cu for CO reduction to ethylene/ethanol [59], Fe/Rh for $N_2$ reduction to ammonia [60], or Co for $O_2$ reduction [61] reactions.

## 4. Conclusion

In summary, we developed an in-situ and one-step strategy to maximize the formation of triple-phase interfaces as catalytic active sites, enhance catalyst utilization, and avoid complete wetting the catalyst layer which leads to pore blockage and unselective $CO_2RR$. Unlike other wettability regulations on the bulk catalyst or the catalyst layer, this method results in the creation of two regions with different wetting features, and the electrolytes can be contained within the hydrophilic region. Compared to the untreated electrodes, the HFGDE treated with 15 s of anodic voltage at 2.0 V exhibited three times higher partial current density of formate (148 mA cm$^{-2}$), outperforming other Bi-based GDEs in the neutral electrolyte (0.5 M KHCO$_3$). This is due to the coexistence of the Cassie-Wenzel state at which highly active reaction zones are formed near solid-liquid-gas interfaces, resulting in a favorable microenvironment for $CO_2RR$. Our study offers a versatile method to tune the surface wettability of electrodes with the potential to be applied for a variety of gas-phase electrochemical reactions.

## CRediT authorship contribution statement

H.R. and L.G. conceived the idea and designed the research. H.R., J. Z. and X.Z. conducted the experiments and characterizations. L.G. conceived the idea and assisted H.R. in the writing and analysis of the data. H.R., L.G. and M.L. contributed to the interpretation of the electrochemical data and characterizations. S.S., T.R., Z.Z., and H.W. provided the use of facilities and advised on the experiments and writing. H. R., L.G., S.H. and Z.Y. co-wrote the manuscript. All authors discussed the results and contributed to the revision of the manuscript at all stages.

## Declaration of Competing Interest

The authors declare that they have no known competing financial interests or personal relationships that could have appeared to influence the work reported in this paper.

## Acknowledgments

## Appendix A. Supporting information

Supplementary data associated with this article can be found in the online version at doi:10.1016/j.apcatb.2022.121362.

## References

[1] H. Shin, K.U. Hansen, F. Jiao, Techno-economic assessment of low-temperature carbon dioxide electrolysis, Nat. Sustain. 4 (2021) 911–919.

[2] L. Xie, J. Liang, C. Priest, T. Wang, D. Ding, G. Wu, Q. Li, Engineering the atomic arrangement of bimetallic catalysts for electrochemical $CO_2$ reduction, Chem. Commun. 57 (2021) 1839–1854.

[3] G. Wang, J. Chen, Y. Ding, P. Cai, L. Yi, Y. Li, C. Tu, Y. Hou, Z. Wen, L. Dai, Electrocatalysis for $CO_2$ conversion: from fundamentals to value-added products, Chem. Soc. Rev. 50 (2021) 4993–5061.

[4] M.T. Tang, H. Peng, P.S. Lamoureux, M. Bajdich, F. Abild-Pedersen, From electricity to fuels: descriptors for C1 selectivity in electrochemical $CO_2$ reduction, Appl. Catal. B 279 (2020) 119384–119394.

[5] J. Zeng, M.R. Fiorentin, M. Fontana, M. Castellino, F. Risplendi, A. Sacco, G. Cicero, M.A. Farkhondehfal, F. Drago, C.F. Pirri, Novel insights into Sb-Cu catalysts for electrochemical reduction of $CO_2$, Appl. Catal. B 306 (2022) 121089–121100.

[6] E.W. Lees, B.A.W. Mowbray, F.G.L. Parlane, C.P. Berlinguette, Gas diffusion electrodes and membranes for $CO_2$ reduction electrolysers, Nat. Rev. Mater. 7 (2022) 55–64.

[7] H. Rabiee, L. Ge, X. Zhang, S. Hu, M. Li, Z. Yuan, Gas diffusion electrodes (GDEs) for electrochemical reduction of carbon dioxide, carbon monoxide, and dinitrogen to value-added products: a review, Energy Environ. Sci. 14 (2021) 1959–2008.

[8] M.R. Li, M.N. Idros, Y.M. Wu, S. Garg, S. Gao, R.J. Lin, H. Rabiee, Z.H. Li, L. Ge, T. E. Rufford, Z.H. Zhu, L.Y. Li, G. Wang, Unveiling the effects of dimensionality of tin oxide-derived catalysts on $CO_2$ reduction by using gas-diffusion electrodes, React. Chem. Eng. 6 (2021) 345–352.

[9] L. Xiao, S. Zhu, Y. Liang, Z. Li, S. Wu, S. Luo, C. Chang, Z. Cui, Effects of hydrophobic layer on selective electrochemical nitrogen fixation of self-supporting nanoporous Mo4P3 catalyst under ambient conditions, Appl. Catal. B 286 (2021) 119895–119906.

[10] I. Merino-Garcia, L. Tinat, J. Albo, M. Alvarez-Guerra, A. Irabien, O. Durupthy, V. Vivier, C.M. Sánchez-Sánchez, Continuous electroconversion of $CO_2$ into formate using 2 nm tin oxide nanoparticles, Appl. Catal. B 297 (2021) 120447–120457.

[11] L. Ge, H. Rabiee, M. Li, S. Subramanian, Y. Zheng, J.H. Lee, T. Burdyny, H. Wang, Electrochemical $CO_2$ reduction in membrane-electrode assemblies, Chem 8 (2022) 663–692.

[12] J. Li, G.X. Chen, Y.Y. Zhu, Z. Liang, A. Pei, C.L. Wu, H.X. Wang, H.R. Lee, K. Liu, S. Chu, Y. Cui, Efficient electrocatalytic $CO_2$ reduction on a three-phase interface, Nat. Catal. 1 (2018) 592–600.

[13] R. Kas, K.K. Hummadi, R. Kortlever, P. de Wit, A. Milbrat, M.W. Luiten-Olieman, N. E. Benes, M.T. Koper, G. Mul, Three-dimensional porous hollow fibre copper electrodes for efficient and high-rate electrochemical carbon dioxide reduction, Nat. Commun. 7 (2016) 10748–10754.

[14] B. Wei, Y.S. Xiong, Z.Y. Zhang, J.H. Hao, L.H. Li, W.D. Shi, Efficient electrocatalytic reduction of $CO_2$ to HCOOH by bimetallic In-Cu nanoparticles with controlled growth facet, Appl. Catal. B: Environ. 283 (2021) 119646–119656.

[15] L. Peng, Y. Wang, Y. Wang, N. Xu, W. Lou, P. Liu, D. Cai, H. Huang, J. Qiao, Separated growth of Bi-Cu bimetallic electrocatalysts on defective copper foam for highly converting $CO_2$ to formate with alkaline anion-exchange membrane beyond KHCO3 electrolyte, Appl. Catal. B: Environ. 288 (2021) 120003–120011.

[16] D. Li, L. Huang, Y. Tian, T. Liu, L. Zhen, Y. Feng, Facile synthesis of porous Cu-Sn alloy electrode with prior selectivity of formate in a wide potential range for CO2 electrochemical reduction, Appl. Catal. B: Environ. 292 (2021) 120119–120129.

[17] H. Rabiee, X. Zhang, L. Ge, S. Hu, M. Li, S. Smart, Z. Zhu, Z. Yuan, Tuning the Product Selectivity of the Cu Hollow Fiber Gas Diffusion Electrode for Efficient $CO_2$ Reduction to Formate by Controlled Surface Sn Electrodeposition, ACS Appl. Mater. Interfaces 12 (2020) 21670–21681.

[18] H. Rabiee, L. Ge, X. Zhang, S. Hu, M. Li, S. Smart, Z. Zhu, H. Wang, Z. Yuan, Stand-alone asymmetric hollow fiber gas-diffusion electrodes with distinguished bronze phases for high-efficiency $CO_2$ electrochemical reduction, Appl. Catal. B: Environ. 298 (2021) 120538–120548.

[19] Y. Wang, Y. Chen, Y. Zhao, J. Yu, J. Liu, Y. Shi, H. Liu, X. Li, W. Zhou, Laser-fabricated channeled Cu6Sn5/Sn as electrocatalyst and gas diffusion electrode for efficient $CO_2$ electroreduction to formate, Appl. Catal. B: Environ. (2021), 120991.

[20] H. Rabiee, L. Ge, X. Zhang, S. Hu, M. Li, S. Smart, Z. Zhu, Z. Yuan, Shape-tuned electrodeposition of bismuth-based nanosheets on flow-through hollow fiber gas diffusion electrode for high-efficiency $CO_2$ reduction to formate, Appl. Catal. B: Environ. 286 (2021) 119945–119956.

[21] M. Duarte, B. De Mot, J. Hereijgers, T. Breugelmans, Electrochemical Reduction of $CO_2$: effect of convective $CO_2$ supply in gas diffusion electrodes, ChemElectroChem 6 (2019) 5596–5602.

[22] H.-Q. Liang, S. Zhao, X.-M. Hu, M. Ceccato, T. Skrydstrup, K. Daasbjerg, Hydrophobic copper interfaces boost electroreduction of carbon dioxide to ethylene in water, ACS Catal. 11 (2021) 958–966.

[23] K. Yang, R. Kas, W.A. Smith, T. Burdyny, Role of the carbon-based gas diffusion layer on flooding in a gas diffusion electrode cell for electrochemical $CO_2$ reduction, ACS Energy Lett. 6 (2020) 33–40.

[24] P. Yue, Q. Fu, J. Li, L. Zhang, L. Xing, Z. Kang, Q. Liao, X. Zhu, Triple-phase electrocatalysis for the enhanced CO$_2$ reduction to HCOOH on a hydrophobic surface, Chem. Eng. J. 405 (2021) 126975–126983.

[25] R. Shi, J. Guo, X. Zhang, G.I.N. Waterhouse, Z. Han, Y. Zhao, L. Shang, C. Zhou, L. Jiang, T. Zhang, Efficient wettability-controlled electroreduction of CO$_2$ to CO at Au/C interfaces, Nat. Commun. 11 (2020) 3028–3037.

[26] Z. Zhao, M.D. Hossain, C. Xu, Z. Lu, Y.-S. Liu, S.-H. Hsieh, I. Lee, W. Gao, J. Yang, B.V. Merinov, W. Xue, Z. Liu, J. Zhou, Z. Luo, X. Pan, F. Zaera, J. Guo, X. Duan, W. A. Goddard, Y. Huang, Tailoring a three-phase microenvironment for high-performance oxygen reduction reaction in proton exchange membrane, Fuel Cells Matter 3 (2020) 1774–1790.

[27] M.E. Leonard, L.E. Clarke, A. Forner-Cuenca, S.M. Brown, F.R. Brushett, Investigating electrode flooding in a flowing electrolyte, gas-fed carbon dioxide electrolyzer, ChemSusChem 13 (2020) 400–411.

[28] J.E. Huang, F. Li, A. Ozden, A. Sedighian Rasouli, F.P. Garcia de Arquer, S. Liu, S. Zhang, M. Luo, X. Wang, Y. Lum, Y. Xu, K. Bertens, R.K. Miao, C.T. Dinh, D. Sinton, E.H. Sargent, CO$_2$ electrolysis to multicarbon products in strong acid, Science 372 (2021) 1074–1078.

[29] C. Kim, J.C. Bui, X. Luo, J.K. Cooper, A. Kusoglu, A.Z. Weber, A.T. Bell, Tailored catalyst microenvironments for CO$_2$ electroreduction to multicarbon products on copper using bilayer ionomer coatings, Nat. Energy 6 (2021) 1026–1034.

[30] T.H.M. Pham, J. Zhang, M. Li, T.H. Shen, Y. Ko, V. Tileli, W. Luo, A. Züttel, Enhanced electrocatalytic CO$_2$ reduction to C2+ products by adjusting the local reaction environment with polymer binders, Adv. Energy Mater. (2022) 2103663–2103672.

[31] J. Wang, T. Cheng, A.Q. Fenwick, T.N. Baroud, A. Rosas-Hernandez, J.H. Ko, Q. Gan, W.A. Goddard III, R.H. Grubbs, Selective CO$_2$ electrochemical reduction enabled by a tricomponent copolymer modifier on a copper surface, J. Am. Chem. Soc. 143 (2021) 2857–2865.

[32] C. Cuevas, D. Kim, K.P. Katuri, P. Saikaly, S.P. Nunes, Electrochemically active polymeric hollow fibers based on poly(ether-b-amide)/carbon nanotubes, J. Membr. Sci. 545 (2018) 323–328.

[33] S. Chen, S. Perathoner, C. Ampelli, H. Wei, S. Abate, B. Zhang, G. Centi, Direct synthesis of ammonia from N2 and H2O on different iron species supported on carbon nanotubes using a gas-phase electrocatalytic flow reactor, ChemElectroChem 7 (2020) 3028–3037.

[34] B. Bian, M.F. Alqahtani, K.P. Katuri, D.F. Liu, S. Bajracharya, Z.P. Lai, K. Rabaey, P. E. Saikaly, Porous nickel hollow fiber cathodes coated with CNTs for efficient microbial electrosynthesis of acetate from CO$_2$ using Sporomusa ovata, ⭧, J. Mater. Chem. A 6 (2018) 17201–17211.

[35] A. Vasileff, C. Xu, L. Ge, Y. Zheng, S.Z. Qiao, Bronze alloys with tin surface sites for selective electrochemical reduction of CO$_2$, Chem. Commun. 54 (2018) 13965–13968.

[36] E. Pajootan, M. Arami, Structural and electrochemical characterization of carbon electrode modified by multi-walled carbon nanotubes and surfactant, Electrochim. Acta 112 (2013) 505–514.

[37] M. Pavese, S. Musso, S. Bianco, M. Giorcelli, N. Pugno, An analysis of carbon nanotube structure wettability before and after oxidation treatment, J. Phys.: Condens. Matter 20 (2008) 474206–474212.

[38] Z. Wang, L. Ci, L. Chen, S. Nayak, P.M. Ajayan, N. Koratkar, Polarity-dependent electrochemically controlled transport of water through carbon nanotube membranes, Nano Lett. 7 (2007) 697–702.

[39] J.M. Simmons, B.M. Nichols, S.E. Baker, M.S. Marcus, O.M. Castellini, C.S. Lee, R. J. Hamers, M.A. Eriksson, Effect of ozone oxidation on single-walled carbon nanotubes, J. Phys. Chem. B 110 (2006) 7113–7118.

[40] D. Wu, G. Huo, W. Chen, X.-Z. Fu, J.-L. Luo, Boosting formate production at high current density from CO$_2$ electroreduction on defect-rich hierarchical mesoporous Bi/Bi2O3 junction nanosheets, Appl. Catal. B: Envrion. 271 (2020) 118957–118964.

[41] G. Gao, M. Pan, C.D. Vecitis, Effect of the oxidation approach on carbon nanotube surface functional groups and electrooxidative filtration performance, ⭧, J. Mater. Chem. A 3 (2015) 7575–7582.

[42] N. Lazouski, M. Chung, K. Williams, M.L. Gala, K. Manthiram, Non-aqueous gas diffusion electrodes for rapid ammonia synthesis from nitrogen and water-splitting-derived hydrogen, Nat. Catal. 3 (2020) 463–469.

[43] F.P. Garcia de Arquer, C.T. Dinh, A. Ozden, J. Wicks, C. McCallum, A.R. Kirmani, D.H. Nam, C. Gabardo, A. Seifitokaldani, X. Wang, Y.C. Li, F. Li, J. Edwards, L. J. Richter, S.J. Thorpe, D. Sinton, E.H. Sargent, CO$_2$ electrolysis to multicarbon products at activities greater than 1 A cm(-2), Science 367 (2020) 661–666.

[44] M.R. Li, M.N. Idros, Y.M. Wu, T. Burdyny, S. Garg, X.S. Zhao, G. Wang, T. E. Rufford, The role of electrode wettability in electrochemical reduction of carbon dioxide, ⭧, J. Mater. Chem. A 9 (2021) 19369–19409.

[45] D. Wu, X. Wang, X.-Z. Fu, J.-L. Luo, Ultrasmall Bi nanoparticles confined in carbon nanosheets as highly active and durable catalysts for CO$_2$ electroreduction, Appl. Catal. B 284 (2021) 119723–119732.

[46] S. Liu, X.F. Lu, J. Xiao, X. Wang, X.W.D. Lou, Bi2 O3 nanosheets grown on multi-channel carbon matrix to catalyze efficient CO$_2$ electroreduction to HCOOH, Angew. Chem. Int. Ed. 58 (2019) 13828–13833.

[47] M. Li, J. Wang, P. Li, K. Chang, C. Li, T. Wang, B. Jiang, H. Zhang, H. Liu, Y. Yamauchi, N. Umezawa, J. Ye, Mesoporous palladium–copper bimetallic electrodes for selective electrocatalytic reduction of aqueous CO2to CO, ⭧, J. Mater. Chem. A 4 (2016) 4776–4782.

[48] Y. Chen, M.W. Kanan, Tin oxide dependence of the CO$_2$ reduction efficiency on tin electrodes and enhanced activity for Tin/Tin oxide thin-film catalysts, J. Am. Chem. Soc. 134 (2012) 1986–1989.

[49] S. Zhang, P. Kang, T.J. Meyer, Nanostructured tin catalysts for selective electrochemical reduction of carbon dioxide to formate, J. Am. Chem. Soc. 136 (2014) 1734–1737.

[50] D. Li, J. Wu, T.T. Liu, J. Liu, Z.Y. Yan, L. Zhen, Y.J. Feng, Tuning the pore structure of porous tin foam electrodes for enhanced electrochemical reduction of carbon dioxide to formate, Chem. Eng. J. 375 (2019) 122024–122032.

[51] A. Salehi-Khojin, H.-R.M. Jhong, B.A. Rosen, W. Zhu, S. Ma, P.J.A. Kenis, R. I. Masel, Nanoparticle silver catalysts that show enhanced activity for carbon dioxide electrolysis, J. Phys. Chem. C 117 (2013) 1627–1632.

[52] F. Lei, W. Liu, Y. Sun, J. Xu, K. Liu, L. Liang, T. Yao, B. Pan, S. Wei, Y. Xie, Metallic tin quantum sheets confined in graphene toward high-efficiency carbon dioxide electroreduction, Nat. Commun. 7 (2016) 12697.

[53] K. Fan, Y. Jia, Y. Ji, P. Kuang, B. Zhu, X. Liu, J. Yu, Curved surface boosts electrochemical CO$_2$ reduction to formate via bismuth nanotubes in a wide potential window, ACS Catal. 10 (2019) 358–364.

[54] X. Ma, J. Tian, M. Wang, M. Shen, L. Zhang, Polymeric carbon nitride supported Bi nanoparticles as highly efficient CO$_2$ reduction electrocatalyst in a wide potential range, J. Colloid Interface Sci. 608 (2022) 1676–1684.

[55] Z. Chen, X. Zhang, W. Liu, M. Jiao, K. Mou, X. Zhang, L. Liu, Amination strategy to boost the CO$_2$ electroreduction current density of M–N/C single-atom catalysts to the industrial application level, Energy Environ. Sci. 14 (2021) 2349–2356.

[56] X. Wang, F. Li, W.-J. Yin, Y. Si, M. Miao, X. Wang, Y. Fu, Atomically dispersed Sn modified with trace sulfur species derived from organosulfide complex for electroreduction of CO$_2$, Appl. Catal. B: Environ. 304 (2022) 120936–120945.

[57] Q. Zhang, Y. Zhang, J. Mao, J. Liu, Y. Zhou, D. Guay, J. Qiao, Electrochemical reduction of CO$_2$ by SnOx nanosheets anchored on multiwalled carbon nanotubes with tunable functional groups, ChemSusChem 12 (2019) 1443–1450.

[58] M.-Y. Lee, S. Ringe, H. Kim, S. Kang, Y. Kwon, Electric field mediated selectivity switching of electrochemical CO$_2$ reduction from formate to CO on carbon supported Sn, ACS Energy Lett. 5 (2020) 2987–2994.

[59] C.W. Li, J. Ciston, M.W. Kanan, Electroreduction of carbon monoxide to liquid fuel on oxide-derived nanocrystalline copper, Nature 508 (2014) 504–507.

[60] B.H.R. Suryanto, C.S.M. Kang, D. Wang, C. Xiao, F. Zhou, L.M. Azofra, L. Cavallo, X. Zhang, D.R. MacFarlane, Rational electrode–electrolyte design for efficient ammonia electrosynthesis under ambient conditions, ACS Energy Lett. 3 (2018) 1219–1224.

[61] A.B.A.A. Nassr, T. Kottakkat, M. Bron, A simple microwave process for the preparation of cobalt oxide nanoparticles supported on carbon nanotubes for electrocatalytic applications, J. Solid State Electrochem. 24 (2019) 131–136.